Frequency-Dependent Capacitance of the Apical Membrane of Frog Skin: Dielectric Relaxation Processes

Mouhamed S. Awayda,* Willy Van Driessche,# and Sandy I. Helman*
*Department of Molecular and Integrative Physiology, University of Illinois at Urbana-Champaign, Urbana, Illinois 61801 USA, and #Laboratory of Physiology, Katholieke Universiteit Leuven, Campus Gasthuisberg, B-3000 Leuven, Belgium

ABSTRACT Impedance analysis of the isolated epithelium of frog skin (northern *Rana pipiens*) was carried out in the frequency range between 0.1 Hz and 5.5 kHz while Na^+ transport was abolished. Under these conditions, the impedance is determined almost completely by the dielectric properties of the apical membranes of the cells and the parallel shunt resistance. The modeling of the apical membrane impedance function required the inclusion of dielectric relaxation processes as originally described by Cole and Cole (1941. *J. Chem. Phys.* 9:341–351), where each process is characterized by a dielectric increment, relaxation frequency, and power law dependence. We found that the apical plasma membrane exhibited several populations of audio frequency dielectric relaxation processes centered at 30, 103, 2364, and 6604 Hz, with mean capacitive increments of 0.72, 1.00, 0.88, and 0.29 $\mu F/cm^2$, respectively, that gave rise to dc capacitances of 1.95 ± 0.06 $\mu F/cm^2$ in 49 tissues. Capacitance was uncorrelated with large ranges of parallel shunt resistance and was not changed appreciably within minutes by K^+ depolarization and hence a decrease in basolateral membrane resistance. A significant linear correlation existed between the dc capacitance and Na^+ transport rates measured as short-circuit currents ($C_a^{dc} = 0.028\ I_{sc} + 1.48$; I_{sc} between 4 and 35 $\mu A/cm^2$) before inhibition of transport by amiloride and substitution of all Na^+ with NMDG (*N*-methyl-D-glucamine) in the apical solution. The existence of dominant audio frequency capacitive relaxation processes complicates and precludes unequivocal interpretation of changes of capacitance in terms of membrane area alone when capacitance is measured at audio frequencies.

INTRODUCTION

The measurement of membrane capacitance has been used widely in biological experiments as a means of assessing changes in membrane area. Such measurements have been of particular interest in studies of epithelial transport, as it has been surmised that regulation of salt and water transport at apical and basolateral membranes of polarized epithelial cells involves targeting and trafficking of channels and transporters between the cytosol and the plasma membranes of the cells.

It is usually assumed that the dielectric properties of the plasma membranes are constant, so that changes in capacitance can be attributed to changes in membrane area. There is, however, an extensive literature dating from the classical papers of Debye (1929), Cole and Cole (1941), and others (see references in Schwan, 1957; Daniel, 1967; Cole, 1968; Gabler, 1978; Pethig, 1979; Jonscher, 1983; Kell and Harris, 1985; Takashima, 1989) that describes the behavior of dipoles in viscous media and documents the existence of audio frequency dielectric dispersions or relaxation processes. Schwan referred to these relaxation processes with the terminology "α- and β-dispersions," where α-dispersions occurred at frequencies below ~100 kHz (Schwan, 1957). To our knowledge, there have been few attempts to determine whether α-dispersions exist in epithelial plasma membranes in general (Watanabe et al., 1991), and no attempts for tight epithelia like those of renal distal tubules.

Our laboratories have been interested in determining the way in which tight epithelia regulate the density of apical membrane epithelial Na^+ channels (ENaCs) and knowing when and under what conditions vesicle trafficking plays a role in shuttling channels between the cytosol and the apical membrane of the cells. In this regard it would be crucial to know whether this membrane exhibits α-dispersions, because their existence would seriously complicate the design of experiments and interpretation of data where changes of capacitance may not reflect alone changes of membrane area.

We have examined with dielectric spectroscopy the native apical membrane of the well-studied frog skin (northern *R. pipiens*), as this membrane contains highly selective and amiloride-sensitive ENaCs. We describe the methods and approaches that we used to determine the complex capacitance of this membrane and report that this plasma membrane exhibits several dielectric relaxation processes at low audio frequencies (<10 kHz) that can be characterized by their capacitive increments, relaxation frequencies, and Cole-Cole power law dependence. An examination of the relationship between the spontaneous rates of Na^+ transport among tissues as measured by short-circuit currents and the dc capacitance indicated that increases in Na^+ transport were correlated with increases in dc capacitance. Further

Received for publication 26 February 1998 and in final form 1 October 1998.

Address reprint requests to Dr. Sandy I. Helman, Department of Molecular and Integrative Physiology, University of Illinois at Urbana-Champaign, 524 Burrill Hall, 407 S. Goodwin Avenue, Urbana, IL 61801. Tel.: 217-333-7913; Fax: 217-333-1133; E-mail: s-helman@uiuc.edu.

Dr. Awayda's present address is Department of Medicine, Section of Gastroenterology, School of Medicine, 1430 Tulane Avenue, Tulane University Medical Center, New Orleans, LA 70112-2699.

0006-3495/99/01/219/14 $2.00

examination of the data revealed that increases in dc capacitance were due to selective increases in the lowest audio frequency capacitive increments of the complex capacitance spectrum and their associated static capacitances. However, it remains unknown from capacitance measurements alone whether changes in capacitance are attributable to changes in membrane area associated with changes in dielectric increments.

Preliminary results have been presented at meetings of the Federation of American Societies of Experimental Biology (FASEB) and the Biophysical Society (Awayda et al., 1989, 1991; Awayda and Helman, 1990, 1992).

BACKGROUND AND THEORETICAL CONSIDERATIONS

Dielectric dispersions

Dielectric dispersions have been observed between subaudio and gigahertz frequencies (Schwan, 1957; Coster and Smith, 1974). By the early part of this century it was widely recognized that dispersions could arise from series structural arrangements of leaky dielectrics that are referred to as Maxwell-Wagner dispersions. In 1929, Debye published his theory of behavior of polar molecules or dipoles in a viscous medium whereby dispersions could also arise from dipolar relaxation processes (Debye, 1929). Cole and Cole (1941) and others examined this theory in a wide range of materials, including biological membranes, and observed dielectric dispersions at audio frequencies. Cole and Cole noted quite generally that dielectric dispersions deviate from ideal behavior, exhibiting a power-law dependence resulting in observation of "depressed" semicircles in Nyquist plots of the complex dielectric constant (ϵ^*) and hence the complex capacitance (C^*). Accordingly, $C^* = \epsilon^* A/d$, where A and d are membrane area and thickness, respectively. Dispersions take the form described by Eq. 1, where for a membrane containing a single dispersion with time constant τ and Cole-Cole power-law factor $\gamma \equiv (1 - \alpha)$,

$$C^* = \left[\frac{\epsilon_0 - \epsilon_\infty}{1 + (j\omega\tau)^{(1-\alpha)}} + \epsilon_\infty\right]\frac{A}{d} \quad (1)$$

which can be rewritten as

$$C^* = \left[\frac{\epsilon_r}{1 + (j\omega\tau_r)^{\gamma_r}}\right]\frac{A}{d} + C_\infty \quad (2)$$

The angular relaxation frequency is $2\pi f_r = 1/\tau_r$, and f_r is the relaxation frequency in Hz. $\epsilon_r = \epsilon_0 - \epsilon_\infty$ is the dielectric increment between infinite and zero frequencies ($\omega = 2\pi f$), where the terminology "infinite frequency" takes on the meaning $f \gg f_r$.

Dispersions at relaxation frequencies less than ~100 kHz have been referred to as α-dispersions. Dispersions at higher radio frequencies have been referred to by Schwan and his colleagues as β-dispersions. γ-Dispersions extend into the gigahertz range (Schwan, 1957; Schwan and Foster, 1980; Foster and Schwan, 1989). Recognizing that multiple dispersions may exist within α, β, γ and higher ranges of frequency, Eq. 2 can be written as Eq. 3 to indicate the possible existence of several capacitive increments $C_{\alpha i}$ and $C_{\beta j}$ associated with the ranges of frequency of the α- and β-dispersions, respectively:

$$C^* = \sum_{i=1}^{n} \frac{C_{\alpha i}}{1 + (j\omega\tau_{\alpha i})^{\gamma_i}} + \sum_{j=1}^{m} \frac{C_{\beta j}}{1 + (j\omega\tau_{\beta j})^{\delta_j}} + C_\beta^\infty \quad (3)$$

At zero frequency, $C^{dc} = \Sigma C_{\alpha i} + \Sigma C_{\beta j} + C_\beta^\infty$. In addition to the static dc capacitance (C^{dc}), we can define static capacitances C_β^∞ and C_α^∞ (see Fig. 1), where $C_\alpha^\infty = \Sigma C_{\beta j} + C_\beta^\infty$ if multiple dispersions exist in the β-range of relaxation frequencies. Accordingly, $C^{dc} = \Sigma C_{\alpha i} + C_\alpha^\infty$ if multiple

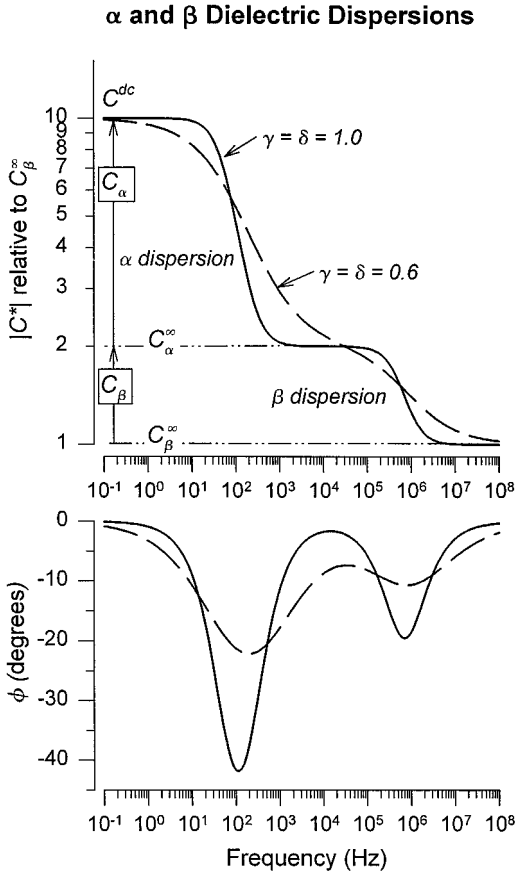

FIGURE 1 Frequency-dependent complex capacitance (C^*) due to α- and β-dielectric dispersions (relaxation processes). Absolute magnitude and phase angle of C^* are plotted against frequency according to Eq. 3 (see text). Curves were calculated assuming relaxation frequencies of 50 Hz and 500 kHz with capacitive increments C_α and C_β in the audio and radio frequency ranges, respectively. C^{dc} is the static *dc* capacitance. C_α^∞ is the static capacitance at frequencies considerably higher than α-relaxation processes but at frequencies considerably less than β-relaxation processes. C_β^∞ is the static capacitance at frequencies considerably greater than β-relaxation processes but less than those at very high frequencies ranging into gigahertz frequencies. The solid lines were calculated assuming ideal Debye dispersions, and the dashed lines were calculated assuming Cole-Cole power law behavior.

dispersions exist in the α-range of relaxation frequencies, which is the focus of attention in the present series of experiments.

Illustrated in Fig. 1 are plots of the magnitude and phase angle (Bode plots) of C^*, where it is assumed for simplicity that α- and β-dispersion ranges of frequency each contain a single relaxation process with ideal Debye ($\gamma = \delta = 1.0$) or Cole-Cole ($\gamma = \delta = 0.6$) power-law behavior. The static capacitance C_β^∞ was assumed to be unity with capacitive increments of 1 and 8 units for β- and α-relaxation processes, respectively, so that C^{dc} is 10 times greater than the static capacitance C_β^∞, and C_α^∞ is two times greater than C_β^∞. Because C^* is complex it can be represented by its real (*Real*) and imaginary (*Imag*) components or by its absolute magnitude $|C^*|$ and phase angle (ϕ). $|C^*|$ and ϕ (degrees) are plotted in Fig. 1.

The theoretical curves in Fig. 1 are also replotted in Fig. 2 *A* in the form of Nyquist plots (*Real* versus *Imag*), where each dispersion gives rise to either an ideal ($\gamma = 1$) or depressed ($\gamma < 1$) semicircle. If C^* is measured only at audio frequencies (α-dispersions), then as indicated by the solid lines, capacitance would decrease with increasing audio frequency, so that extrapolation of C^* to the real axis would give the static capacitance C_α^∞. The semicircles appear depressed when $\gamma < 1.0$, and this behavior is due presumably to a distribution of time constants or relaxation times of the dipoles associated with the relaxation process (Cole and Cole, 1941; Cole, 1968; Gabler, 1978; Pethig, 1979; Jonscher, 1983). When capacitance is measured at audio frequencies and the membrane contains several α-relaxation processes between C^{dc} and C_α^∞, C^* can be decomposed into a sum of processes as shown in Fig. 2 *B* with capacitive increments $C_1, C_2, \ldots, C_n$ at relaxation frequencies $f_1, f_2, \ldots, f_n$ with static capacitances at the intercepts on the real axis, $C_1^\infty, C_2^\infty, \ldots, C_n^\infty$. Accordingly, $C_n^\infty \equiv C_\alpha^\infty$, and it is implied by omission of the α subscript that our measurements will pertain only to relaxation processes in the range of α-dispersions. Hence the complex capacitance measured in the audio frequency range can vary not only because of changes in membrane area and thickness, but also because of changes in dielectric increments, relaxation frequencies, and the distribution of relaxation times of each of the relaxation processes. We shall in this paper use the terminology "capacitive increments" and "dielectric increments," recognizing that changes in capacitance can occur because of changes in dielectric increments with or without changes in membrane area.

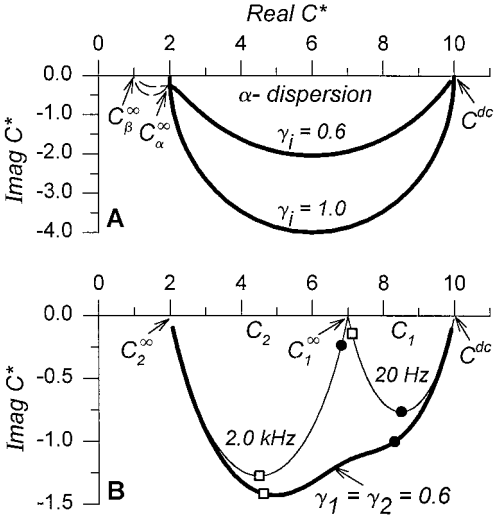

FIGURE 2 Frequency-dependent complex capacitance plotted as Nyquist plots with real (*Real*) against imaginary (*Imag*) components of C^*. Theoretical plots of Fig. 1 are shown in *A*. Static capacitances C^{dc}, C_α^∞, and C_β^∞ are indicated on the real axis. Note depression of the semicircles when the Cole-Cole power law factor is less than unity. Thick solid lines represent the complex capacitance spectrum observable at audio frequencies. (*B*) Two α-relaxation processes with relaxation frequencies of 20 Hz and 2.0 kHz and with capacitive increments C_1 and C_2 of 3 and 5 units, respectively. The C^{dc} as given by Eq. 5 and graphically represented here reflects the sum of the capacitive increments and the static capacitance C_2^∞. At frequencies considerably higher than 2 kHz, the static capacitance C_2^∞ approaches a value of 2 units and would remain unchanged if the area is unchanged and, in particular, if changes occur in either the relaxation frequencies and/or the capacitive increments. Also indicated is the static capacitance C_1^∞ that intercepts the real axis at 7 units. If, for example, the relaxation frequency at 2 kHz is increased to frequencies in the range of MHZ or higher, this very high frequency relaxation process would not be observed at audio frequencies. Instead, the 20-Hz relaxation process would appear as indicated (*thin solid line*) with a capacitive increment C_1 that extrapolates at much higher frequencies to the static capacitance C_1^∞. For points of reference, the solid circles mark frequencies at 20 Hz, and the open squares mark frequencies at 2.0 kHz on the thick solid lines of the capacitance spectrum and on the individual relaxation processes illustrated by the thin solid lines that give rise to the spectrum.

MATERIALS AND METHODS

Experiments were carried out with isolated epithelial preparations of abdominal skins of northern frogs (*Rana pipiens;* Kons Scientific Co., Germantown, WI) devoid of connective tissue and glands of the corium (Fisher et al., 1980). Tissues were mounted in edge-damage-free chambers (Abramcheck et al., 1985), which were continuously perfused with Ringer's solution at a rate of ~5 ml/min. Tissues were short-circuited, except during measurements of the transepithelial impedance, with a four-electrode (Ag/AgCl, 4.5M NaCl, 3% agar) very low-noise voltage clamp.

Impedance analysis

Transepithelial impedance was measured under voltage-clamp conditions at frequencies between 0.1 Hz and 5.5 kHz. The voltage command signals consisted of two bands of 53 discrete frequencies as described by Măргineanu and Van Driessche (1990). Command signals applied to the tissues ranged between ~2 and ~20 mV peak to peak (p-p). Because the measured impedance was independent of the magnitude of the command voltage, it could be inferred that the impedance was measured in linear regions of current-voltage relationships. The low-frequency band contained frequencies between 0.1 and 43.1 Hz, whereas the high-frequency band overlapped the low-frequency band and contained frequencies between 12.8 and 5516 Hz. The command signals were applied to the voltage clamp sequentially. Transepithelial voltage and current signals were acquired with a 12-bit analog-to-digital converter after the signals were filtered at their Nyquist frequencies and amplified. Voltage command signals were also filtered before being applied to the voltage clamp. The digitized current and voltage signals were Fourier transformed to yield current and voltage vectors from which the measured impedance (Z_{meas}) was calculated at each of the 106 discrete frequencies. With a fundamental frequency of 0.1 Hz

for the lower frequency band and a fundamental frequency of 12.8 Hz for the higher frequency band, the time for data acquisition was slightly greater than 10 s. In some experiments, the fundamental frequency of the lower frequency band was increased to 0.2 or 0.5 Hz, thereby shifting the entire lower frequency band to higher frequencies and reducing the time for data acquisition. The results were the same.

The solution resistance (R_{sol}) between the voltage electrodes was measured sometimes before and always at the end of the experiments. Impedance was measured with the electrodes in place, but in the absence of tissue separating apical and basolateral chamber solutions. R_{sol} was independent of frequency (<100 kHz), as expected for simple electrolyte solutions, and averaged 38.9 ± 1.0 $\Omega \cdot cm^2$ for our chambers with 0.484 cm^2 cross-sectional area and the positioning of the voltage electrodes within the chambers. In addition to R_{sol}, cytoplasmic resistance (R_{cyt}) exists in series with apical and basolateral plasma membranes for a combined resistance $R_{ser} = R_{sol} + R_{cyt}$. Assuming a cell layer thickness of 30–60 μm for the electrically coupled basolateral membranes of the multicell layered epithelium of frog skin and a volume resistivity of the Ringer solution of ~100 $\Omega \cdot cm$ of the cytoplasmic fluid, R_{cyt} would be in the range of 0.3–0.6 $\Omega \cdot cm^2$. If cytoplasmic volume resistivity is about twice that of the extracellular solution volume resistivity and in the range reported by Fricke and Morse (1925) and Bao et al. (1992), R_{cyt} is near 1 $\Omega \cdot cm^2$ and is the value we used in our calculations. Accordingly, the transepithelial impedance $Z_T = Z_{meas} - R_{ser}$.

We also examined under current-clamp conditions the Z_{meas} at frequencies between 10 and 100 kHz, using 18-$\mu A/cm^2$ p-p sinusoids, resulting in <2-mV p-p changes in transepithelial voltage. Amplified current and voltage signals were displayed as Lissajous figures on a Nicolet model 2090 digital oscilloscope (Nicolet Instruments Corp., Madison, WI), and the impedance was determined from measurements of photographic images. These data confirmed that the Z_{meas} at much higher frequencies than 5.5 kHz approached those of R_{ser} as indicated above and as expected when the capacitive reactances of apical and basolateral membranes approach zero.

In the absence of tissue, the frequency response (<100 kHz) of the chambers and bridges was purely resistive, so that no correction was required for stray capacitance. The chambers were characterized with Ringer's solution alone and with Lucite gaskets (to replace the tissue) predrilled with small apertures to give values of R_{sol} between 2 and 25 $k\Omega \cdot cm^2$. The phase difference between voltage and current signals was $<\pm 0.1°$ under voltage-clamp conditions and $<\pm 1.5°$ under current-clamp conditions.

Experimental design

Transporting conditions

All experiments reported here began with tissues bathed symmetrically with a sodium sulfate Ringer's solution containing (in mM) 56 Na_2SO_4, 2 $CaSO_4$, and 2.4 $KHCO_3$ (pH ~8.1). (Preliminary experiments were carried out with both chloride- and sulfate-containing Ringer solutions bathing apical and basolateral borders of the tissues and with apical solutions where Na^+ was substituted with either tetramethyl-ammonium or *N*-methyl-D-glucamine (NMDG). Regardless of the presence or absence of 100 μM amiloride in the apical solution in sodium-free solutions, apical membranes exhibited relaxation phenomena that could not be due to the presence of amiloride at these very high concentrations, which ensured essentially complete block of conductance and loss of Na^+ current through amiloride-sensitive epithelial Na^+ channels.) Tissues were short-circuited continuously for 1–2 h to allow the short-circuit current to stabilize. Open-circuit voltages measured just before short-circuiting of the tissues averaged 72.3 ± 3.9 mV (range 33.9–108 mV), and short-circuit currents averaged 16.8 ± 1.3 $\mu A/cm^2$ (range 3.6–34.2 $\mu A/cm^2$) just before inhibition of Na^+ transport. Under transporting conditions, the transepithelial impedance is determined by the series impedance of the apical (Z_a) and basolateral (Z_b) membranes, shunted by a paracellular shunt resistance, R_p (Fig. 3 *A*).

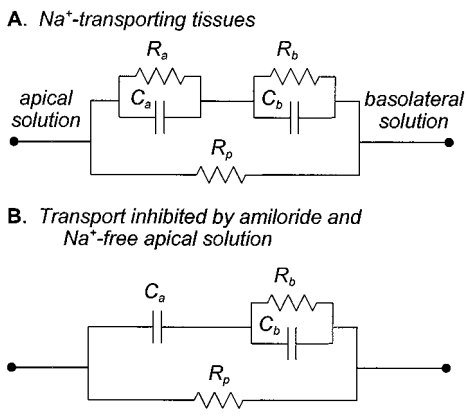

FIGURE 3 Transepithelial electrical equivalent circuits. (*A*) Apical and basolateral membranes are shunted by the paracellular resistance R_p. R_a and R_b are the slope resistances, and C_a and C_b are the capacitances of apical and basolateral membranes, respectively. Not shown is the solution resistance R_{sol} in series with the tissues. (*B*) Inhibition of apical membrane Na^+ entry (100 μM amiloride and substitution of all apical solution Na^+ with NMDG (see text)) cause $R_a \gg R_b$, and thus R_a is negligible. If, in addition, the impedance of basolateral membranes is considerably less than the reactance of the apical membrane capacitance ($C_b \gg C_a$ and/or the decrease in R_b by K^+-depolarization of the basolateral membrane), the transepithelial electrical equivalent circuit reduces to C_a paralleled by R_p.

Transport-inhibited conditions

Apical membranes contain both amiloride-sensitive and amiloride-insensitive channels with very high selectivity for Na^+. In the presence of 100 μM amiloride to inhibit transport through amiloride-sensitive channels and in the complete absence of Na^+ in the apical solution to decrease ionic conductance through blocker-insensitive channels, the apical membrane impedance (Z_a) is reduced electrically to the reactance of the apical membrane capacitance (C_a) (Fig. 3 *B*). At the frequencies of interest, apical membrane resistance, R_a, is considerably larger than the apical membrane capacitive reactance and considerably larger than the basolateral membrane resistance, R_b, which averages near 1000 $\Omega \cdot cm^2$ (Helman and Fisher, 1977, 1982). Because of the functional electrical coupling of the basolateral membranes of the multicellular layers of the skin, the capacitance of the basolateral membranes, C_b, is expected to be considerably larger than C_a by ~30–40 times (considering areas alone), depending in part on the degree of apical and basolateral membrane infolding (see Appendix). Thus the impedance of the basolateral membranes, Z_b, is expected to be quite small and nearly negligible relative to Z_a (see Results). Accordingly, under transport-inhibited conditions, the transepithelial impedance is determined principally at the frequencies of interest by the parallel combination of apical membrane impedance and the shunt resistance, R_p, so that

$$Z_{meas} = \frac{R_p}{1 + j\omega R_p C_a^*} + R_{ser} \quad (4)$$

As the frequency approaches zero, Z_{meas} approaches the series sum of R_p and R_{ser}. R_p averaged 23.6 ± 2.6 $k\Omega \cdot cm^2$ and ranged between 5.0 and 62.4 $k\Omega \cdot cm^2$. I_{sc} was not different from zero when the apical chamber was perfused with 100 μM amiloride (Merck Sharp and Dohme Research Laboratory, Rahway, NJ) containing Ringer's solution, where Na^+ was replaced with NMDG (Sigma Chemical Co., St. Louis, MO).

Calculation of complex capacitance, C_a^*

With the measured impedance and series resistance and with a preliminary estimate of R_p obtained by extrapolation of ($Z_{meas} - R_{ser}$) to zero frequency, C_a^* was calculated (Eq. 4) at each of the 106 discrete frequencies.

This extrapolation to values of R_p could be done by eye or by using TableCurve (Jandel Scientific, San Rafael, CA) to fit the lowest frequency values of *Real* ($Z_{meas} - R_{ser}$) as a function of frequency to smooth curves that intercepted the impedance ordinate at zero frequency. From a direct graphical examination of the Nyquist capacitance plots, we determined not only the number of relaxation processes, but also the approximate magnitudes of the capacitive increments (C_i) and relaxation frequencies (f_r) that were used as the starting values for nonlinear curve fitting of the impedance data. It may be emphasized that the data in all cases conformed to Cole-Cole relaxation processes, and more complicated phenomena could be excluded.

Final determination of the magnitudes of the capacitive increments, relaxation frequencies, and power-law dependencies was done using a least-squares nonlinear minimization program (MINSQ, now called Scientist; Micromath Scientific, Salt Lake City, UT) to minimize the real and imaginary components of Z_{meas} over the parameter space of the relaxation processes and the R_p, where for the α-dispersions,

$$C^* = \sum_{i=1}^{n} \frac{C_i}{1 + (j\omega\tau_i)^{\gamma_i}} + C_\alpha^\infty \qquad (5)$$

It should be emphasized that all data are normalized to the planar area of the tissues. Actual membrane area, depending on the degree of in- and out-foldings, will accordingly be greater than planar area. Accordingly, the ratio of actual to planar area is variable, and this will be reflected in the values of capacitance reported ($\mu F/cm^2$ of planar area) when changes in actual area occur.

Data are summarized as means ± SE unless noted otherwise. All experiments were carried out at room temperature.

RESULTS

Transepithelial impedance of transport-inhibited tissues

Impedance was measured before (see Appendix) and after complete inhibition of Na^+ transport. Illustrated for a typical transport-inhibited tissue in Fig. 4 is the Z_{meas} plotted as a Nyquist plot at frequencies between 0.1 Hz and 5.5 kHz (Fig. 4 *A*) and at frequencies greater than or equal to 43 Hz in expanded form in Fig. 4 *B*. The data are also plotted in Fig. 4, *C* and *D*, in the form of Bode plots. All attempts to fit the data to single ideal semicircles over the entire range of frequency failed. With bandwidth limited to low frequencies (<50 Hz), smooth curves could be fit to the impedance vectors, requiring, however, a power-law dependence to account for flattening or depression of the semicircles. The solid lines shown in Fig. 4 were determined by nonlinear curve fitting of the data between 0.5 Hz and 43 Hz to an equation of a depressed impedance semicircle used previously (Van Driessche, 1986) and modified here (Eq. 6) for transport-inhibited tissues:

$$Z_{meas} = \frac{R_p}{1 + (j\omega R_p C_a)^{(1-\alpha)}} + R_{ser}\Big|_{<50\ Hz} \qquad (6)$$

where it is explicitly assumed that C_a is constant at all frequencies. In every case, $1 - \alpha$ was less than unity

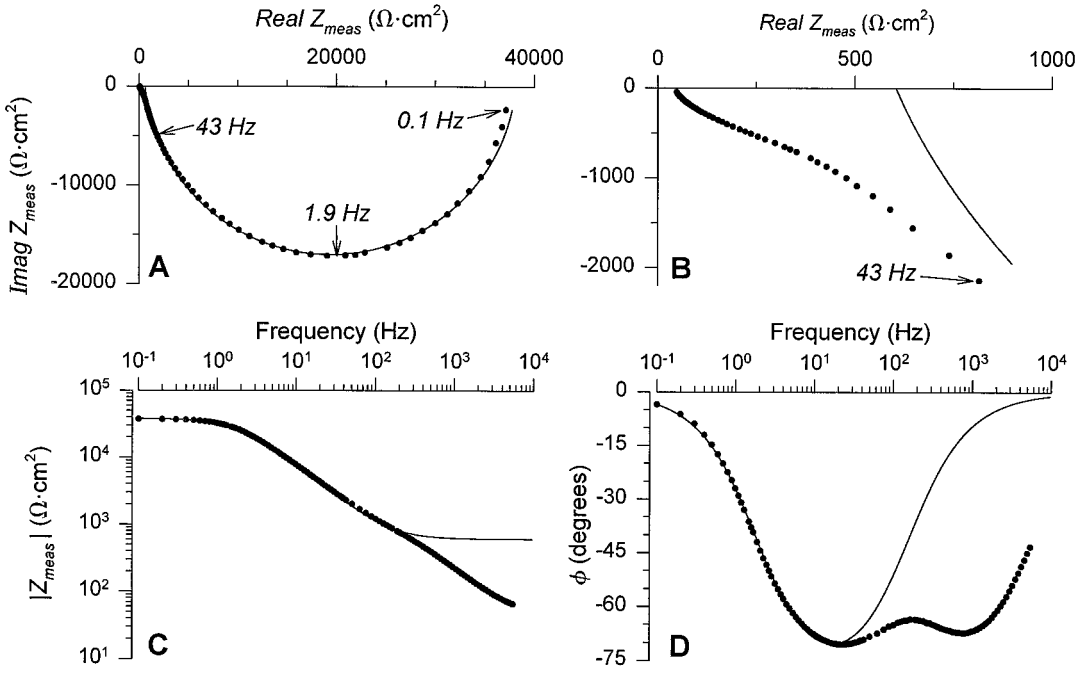

FIGURE 4 Measured impedance (Z_{meas}) of isolated epithelium of frog skin after inhibition of apical membrane Na^+ entry by amiloride and Na^+-free apical solution. (*A*) Nyquist plot of Z_{meas} at frequencies between 0.1 Hz and 5.5 kHz. Shunt resistance, R_p, extrapolated to the real axis is 37.8 $k\Omega \cdot cm^2$. A single depressed semicircle (Eq. 4, *solid line*) was fit to the data between 0.5 Hz and 43 Hz. The apex of the depressed semicircle is at 1.9 Hz. (*B*) Expanded view of Z_{meas} at frequencies ≥ 43 Hz. The solid line is the extension of the depressed semicircle shown in *A*. At 5.5 kHz, Z_{meas} approaches the value of R_{sol}. The real axis intercept of the fitted line exceeds the value of R_{sol}. (*C* and *D*) Bode plots of the absolute value of Z_{meas} and phase angle (ϕ). Solid lines correspond to those in *A* and *B* for a depressed semicircle fitted to data at frequencies between 0.5 and 43 Hz.

(ranging between ~0.80 and ~0.98), indicating depression or power-law dependence of the impedance of transport-inhibited tissues. Similar values of power-law dependence were observed for impedance of tissues studied in their transporting state (see Appendix). Because 1) we could not explain power-law dependence of impedance at very low frequencies less than 50 Hz while assuming constancy of C_a; 2) we could not explain having to exclude data for fitting at frequencies greater than 50 Hz to any model where capacitance is constant; 3) we could not fit data to distributed parameter models consistent with the morphology of this epithelium; and 4) because the theory of dipolar relaxations outlined above could explain power-law dependence of the impedance as well as the more complex behavior of impedance at all frequencies, we rejected the thesis that C_a was constant at audio frequencies.

Apical membrane capacitance is frequency dependent (dielectric spectroscopy)

Apical membrane capacitance, C_a*, calculated as described in Materials and Methods, invariably showed a strong dependence on frequency, as illustrated in Fig. 5. Between 0.1 Hz and 5.5 kHz, capacitance fell progressively with increasing frequency. Inspection of the capacitance spectra indicated clearly that frequency-dependent changes in capacitance were associated with at least two or three relaxation processes, as indicated in the spectra shown in Fig. 5, *A* and *B*. For the spectra shown in this figure, relaxation frequencies were 9.9 Hz, 152 Hz, and 5.8 kHz (Fig. 5 *A*) and 67 Hz and 3.2 kHz (Fig. 5 *B*) with corresponding capacitive increments and static capacitances indicated on the real axis of the Nyquist plots.

A histogram of relaxation frequencies was generated by log binning the relaxation frequencies from all tissues, as indicated in Fig. 6. The histogram was fit by nonlinear curve fitting to the sum of four Gaussian functions characterized in the usual way by their means ± SD. Relaxation frequencies fell into four populations centered at means of 30.4, 103, 2364, and 6604 Hz (Fig. 6 and Table 1), which we labeled $f_1 \ldots f_4$ with corresponding capacitive increments $C_1 \ldots C_4$ (Table 2).

Further inspection of the data revealed that the tissues could be grouped as summarized in Table 1 as groups I and II. Tissues in group I characteristically exhibited relaxation frequencies in the range of f_3, averaging 2085 ± 131 Hz (mean ± SE). Tissues in group II exhibited relaxation frequencies in the range of f_4, averaging 6806 ± 393 Hz. In no tissue did we observe relaxation frequencies in the frequency ranges of both f_3 and f_4. Relaxation frequencies were in the range of either f_3 or f_4.

Each group could be subdivided further, depending on the existence of f_1 and/or f_2, as indicated also in Table 1. Relaxation processes in the ranges of f_1 or f_2 could exist alone or in combination. f_1 averaged 24.8 ± 3.1 Hz, and f_2 averaged 142 ± 16.8 Hz.

Retaining the same groupings, we have summarized in Table 2 C_a^{dc}, C_α^∞, and the capacitive increments C_1, C_2, C_3, and C_4. C_a^{dc} and C_α^∞ averaged 1.95 ± 0.06 and 0.14 ± 0.01 μF/cm^2, respectively, indicating that α-dispersions ac-

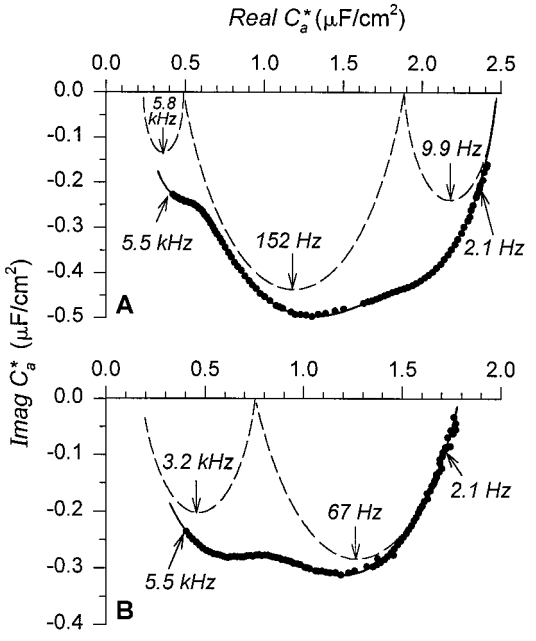

FIGURE 5 Complex capacitance of apical membrane of frog skin (C_a*). Representative examples are shown of apical membranes exhibiting two (*B*) or three (*A*) relaxation processes. (*A*) C^{dc} was near 2.5 μF/cm^2. The solid line represents the nonlinear least-squares best fit of the impedance vectors. Dashed lines represent the individual relaxation processes at frequencies of 9.9 Hz, 152 Hz, and 5.8 kHz. Capacitive increments (C_i) and static capacitances (C_i^∞) are indicated at the intercepts of the depressed semicircles on the real axis. (*B*) C^{dc} was near 1.8 μF/cm^2. Relaxation frequencies of the two processes were 67 Hz and 3.2 kHz, with corresponding capacitive increments and static capacitances indicated on the real axis at the intercepts of the individual relaxation processes (*dashed lines*).

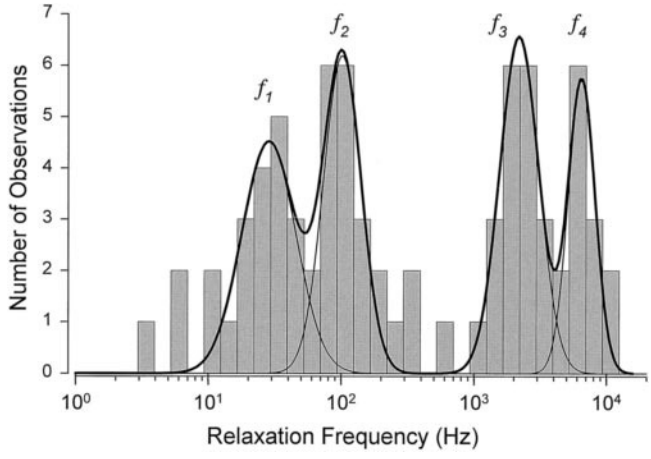

FIGURE 6 Histogram of relaxation frequencies. Observations were log-binned and fit to four populations of relaxation frequencies (f_i), assuming normal Gaussian distributions. Mean relaxation frequencies and standard deviations are summarized in Table 1.

TABLE 1 Relaxation frequencies

	f_1	f_2	f_3	f_4
Population means ± SD	30.4 ± 12.1	103 ± 30	2,364 ± 985	6,604 ± 1,175
Group I				
I A (16)	27.5 ± 2.7	—	1,790 ± 177	—
I B (11)	—	97.7 ± 9.1	2,386 ± 212	—
I C (6)	9.7 ± 3.3	151 ± 48	2,320 ± 318	—
Group II				
II A (2)	32.1 ± 7.9	—	—	7,841 ± 1,677
II B (5)	—	97.6 ± 16.4	—	5,619 ± 310
II C (9)	28.4 ± 9.2	214 ± 37	—	7,235 ± 510
All experiments (49)	24.8 ± 3.1 (33)	142 ± 16.8 (31)	2,085 ± 131 (33)	6,806 ± 393 (16)

Values of relaxation frequencies in groups I and II are means ± SE (Hz). The number of experiments (n) is in parentheses.

counted for ~93% of the static dc capacitance of the tissues. Although there is considerable uncertainty in the absolute values of C_α^∞, owing to the uncertainty of the precise value of the series resistance, and although the absolute area and thickness of the native apical membrane dielectric are unknown, it is of interest to note that with dielectric thicknesses, d, in the range of 40–60 Å, the capacitance of a vacuum (C_{vac}) would be in the range of 0.22–0.15 μF/cm^2 and in the range of the calculated values of C_α^∞ ($C_{vac} = 8.85 \cdot 10^{-14}/d$, Farads/cm^2).

Between groups, the capacitive increment C_3 was greater in value than C_4, averaging 0.88 ± 0.06 and 0.29 ± 0.03 μF/cm^2, respectively. When the capacitive increments C_1 or C_2 were present alone (groups IA and IB; groups IIA and IIB), their values were similar within groups. When C_1 and C_2 were present together in the same spectrum, there appeared to be an inverse relationship between the values of C_1 and C_2 (Fig. 7).

To ensure that the higher frequency relaxation processes did not arise from critical errors in estimation of the series solution resistance, $|Z_{meas}|$ was determined in the range of 10–100 kHz. The values of $|Z_{meas}|$ extrapolated to infinite frequency were found to approach closely those values of R_{sol} measured in the absence of tissue. To ensure viability of the assumption for frog skins that the impedance of the basolateral membranes was negligible under the conditions of our transport-inhibited studies, basolateral membranes were depolarized within seconds by substitution of basolateral solution Na^+ with K^+, which results in marked decreases in R_b and hence Z_b (Tang et al., 1985). The apical membrane dc capacitance remained unchanged from control for 1 h after basolateral membrane depolarization (Fig. 8). Relatively small and slow time-dependent changes in the capacitive increments and relaxation frequencies were observed but were not correlated in time with a decrease in the magnitude of Z_b. No correlation existed between the capacitance spectra and the spontaneous values of the dc shunt resistance (R_p), which ranged between 5.0 and 62.4 k$\Omega \cdot$ cm^2, and the capacitance spectra remained unchanged after needle puncture of the tissues to artificially decrease the dc shunt resistance to low values less than 1 k$\Omega \cdot$ cm^2. Consequently, it was concluded that the observed relaxation processes were attributable to processes associated with the apical membranes of the epithelial cells.

Cole-Cole power-law dependence

Most likely because of distribution of time constants associated with a relaxation process, dielectric dispersions exhibit a power-law dependence that was first recognized by Cole and Cole (1941). γ_i ranged between 0.5 and 1.0 among all relaxation processes and averaged 0.70 ± 0.03, 0.72 ± 0.02, 0.76 ± 0.02, and 0.95 ± 0.02 for the $f_1 \ldots f_4$ relaxation processes, respectively.

TABLE 2 Contribution of capacitive increments to apical membrane capacitance

	Static capacitances		Capacitive increments			
	C_a^{dc}	C_α^∞	C_1	C_2	C_3	C_4
Group I						
I A (16)	1.95 ± 0.10	0.09 ± 0.01	0.78 ± 0.09	—	1.08 ± 0.08	—
I B (11)	1.80 ± 0.13	0.13 ± 0.01	—	0.98 ± 0.12	0.69 ± 0.06	—
I C (6)	2.12 ± 0.08	0.13 ± 0.02	0.28 ± 0.08	1.02 ± 0.18	0.69 ± 0.17	—
Group II						
II A (2)	2.17 ± 0.21	0.16 ± 0.07	1.53 ± 0.25	—	—	0.48 ± 0.03
II B (5)	1.82 ± 0.15	0.22 ± 0.04	—	1.31 ± 0.13	—	0.28 ± 0.05
II C (9)	2.03 ± 0.14	0.22 ± 0.03	0.72 ± 0.12	0.84 ± 0.15	—	0.26 ± 0.03
All experiments (49)	1.95 ± 0.06	0.14 ± 0.01	0.72 ± 0.07	1.00 ± 0.07	0.88 ± 0.06	0.29 ± 0.03

Values of capacitance in μF/cm^2 are means ± SE. The number of observations is in parentheses.

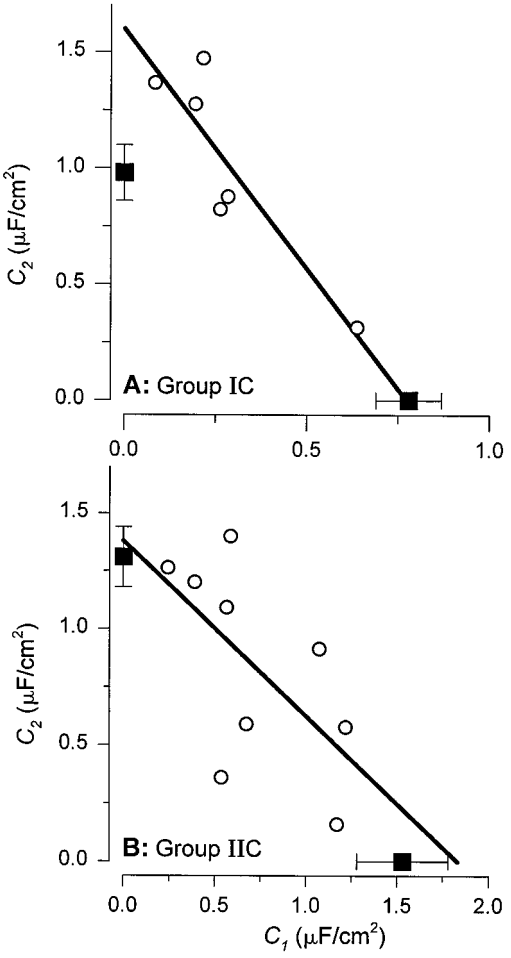

FIGURE 7 Inverse relationship between capacitive increments C_1 and C_2 (○) in tissue groups IC (*A*) and IIC (*B*) summarized in Table 2. Shown also are the means ± SE (■) of C_1 (group IA) and C_2 (group IB) in *A*, and C_1 (group IIA) and C_2 (group IIB) in *B* in those tissues exhibiting either C_1 or C_2 capacitive increments but not both in the same spectrum.

Static dc capacitance varies with short-circuit currents

The static dc capacitance was correlated with the short-circuit currents, which are a measure of the rate of Na^+ entry into the cells through their apical membranes (Fig. 9). Linear regression analysis of the C_a^{dc} plotted as a function of the spontaneous I_{sc} indicated that dc capacitance increased with a slope of 0.028 ± 0.006 (SE) μF/μA and a zero current transport rate intercept of 1.48 ± 0.12 (SE) μF/cm^2.

Contribution of capacitive increments to the static dc capacitance

Because the dc capacitance was correlated with the rate of Na^+ transport, it was of interest to know which of the dielectric increments contributed to increases in the dc capacitance. To address this question, we plotted the capacitive increments as a function of the static dc capacitance that ranged between 1.25 and 2.72 μF/cm^2. As indicated in Fig. 10 *D*, the C_4 capacitive increments (group II tissues) were generally quite small and did not increase significantly with increases in C_a^{dc}. Although the C_3 capacitive increments (group I) varied considerably among tissues, C_3 did not change significantly with increases in the dc capacitance. In contrast, and as indicated in Fig. 10, *A* and *B*, increases in C_a^{dc} could be attributed to increases in C_1 and/or C_2. Accordingly, the transport-related increases in static dc capacitance were due principally to selective increases in the very low frequency C_1 and/or C_2 capacitive increments.

DISCUSSION

Apical membrane electrical equivalent circuit and α-dispersions

In view of the extensive literature documenting the existence of audio frequency α-dispersions in dielectrics, it should not be surprising that a biological plasma membrane like the native apical membrane of frog skin exhibits dielectric relaxation phenomena. We found that ~93% of the static dc capacitance of this membrane was frequency dependent, exhibiting multiple relaxation processes at low and very low audio frequencies. Accordingly, the capacitance of this membrane should be modeled as indicated in Fig. 11 as the parallel sum of capacitive increments (Eq. 5) with time constants $R_iC_i = (2\pi f_i)^{-1}$ associated with each of the relaxation processes. In contrast to the apical membrane resistance R_a that represents the dc or ionic conductance of the epithelial Na^+ channels, the R_i of the dielectric relaxation processes are ac resistances that contribute to the membrane resistance (or conductance) only at frequencies greater than zero. These resistances are referred to as ac resistances because the charges giving rise to the relaxations are constrained to motions within the dielectric and thus do not contribute to the dc conductance of the membrane. With mean f_i and C_i taken from Tables 1 and 2, R_i of the four relaxation processes were calculated, which in sequence $R_1 \ldots R_4$ were 8272, 1189, 84, and 76 $\Omega \cdot cm^2$.

Origin of relaxation processes

In principle, the R_i will depend upon the charge density and mobility of the charges and/or dipoles within the dielectric, and so an equivalent volume resistivity (ρ_i) can be calculated. Assuming a maximum dielectric thickness (d) of 5 nm and a uniform distribution of charges within the dielectric, $\rho_i = R_i/d$. In fact, we do not know how the charges are distributed, and hence ρ_i may be larger than the values summarized in Table 3 if membrane thickness is less than 5 nm. ρ_i ranged between 0.16 and 17.8 M$\Omega \cdot$ cm among relaxation processes approaching, at the lower frequency relaxation frequencies, the volume resistivities of 16–18 M$\Omega \cdot$ cm distilled water, where at neutral pH charge densities would be in the vicinity of 10^{-7} M at aqueous ionic mobilities. Realistically, the mobilities of the dielectric charges are expected to be considerably less than those of an

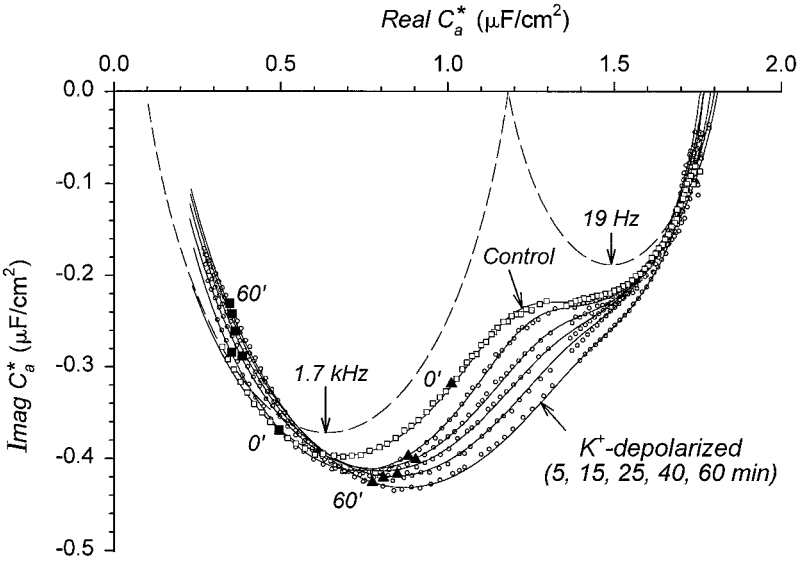

FIGURE 8 Changes in complex capacitance C_a^* after K^+-depolarization of basolateral membranes. The control spectrum (□) consisted of two relaxation processes with relaxation frequencies of 19 Hz and 1.7 kHz. Spectra were measured at 5-min intervals after K^+-depolarization (○) and at 5, 15, 25, 40, and 60 min (shown in this figure). Note absence of change of the dc capacitance and the relatively slow time-dependent changes in capacitance and phase angle at the higher audio frequencies. Relatively small time-dependent increases in the absolute value of capacitance, $|C_a^*|$, at 166.4 Hz (▲) and marked time-dependent decreases at 1062 Hz (■).

aqueous environment, and charge densities would be scaled upward by one or more orders of magnitude, but not to the extent of reaching the molar range of concentration of the lipids. Because the concentration of lipids within the bilayer and the charge densities associated with the relaxation processes are most likely different by several orders of magnitude, it may be inferred that either an extremely small quantity of charged lipids gives rise to α-dispersions, and/or that dispersions may arise from charges associated with the integral transmembrane proteins.

There are no definitive studies that permit unequivocal speculation on the origin of α-dispersions in native biological membranes. In this regard, α-dispersions have not been observed in studies of planar neutral lipid bilayer membranes with or without adsorbed layers of proteins (Hanai et al., 1964, 1965; White and Thompson, 1973). Proteins studied in aqueous solutions give rise to β-dispersions at radio frequencies (Gabler, 1978, and references therein), so it is unlikely that loose protein loops or strands extending from the surfaces of the lipid bilayers can account for the α-dispersions of native plasma membranes. Because a large variety of channels, transporters, and other proteins span the bilipid layers of plasma membranes, it is possible and seems likely that low-frequency α-dispersions may arise from dipoles associated with integral membrane-spanning proteins that are sensed by the electrical field within the membrane. It has also been pointed out, however, that α-dispersions can arise from translational and rotational movements of charged proteins and lipids in vesicles and cells, where unrestricted translation of the lipids and proteins within the plane of the membrane can give rise to low and very low audio frequency dielectric relaxations (Kell and Harris, 1985). It is also well appreciated that dielectric dispersions can arise from charge movements within the membrane that are associated with the gating mechanism of excitable channels in nerve membranes (Armstrong and Bezanilla, 1975).

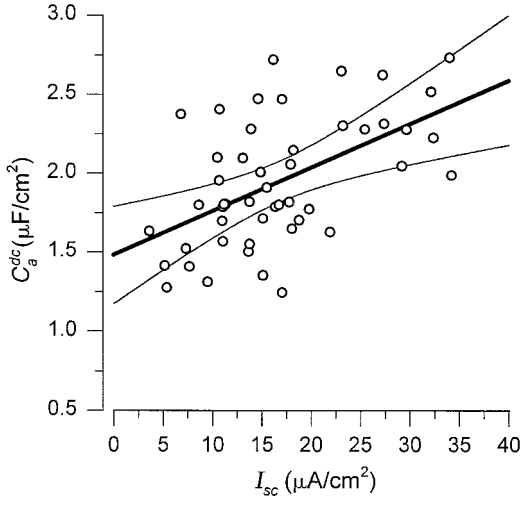

FIGURE 9 Relationship between short-circuit current (I_{sc}) and dc capacitance among all tissues ($n = 49$). The linear regression (——) and the 99% confidence interval (——) are shown. The slope is 0.028 ± 0.006 (SE) μF/μA with zero current intercept 1.48 ± 0.12 (SE) μF/cm². The 99% confidence limits are 0.011 and 0.044 μF/μA for the slope and 1.17 and 1.79 μF/cm² for the intercept.

There has, in fact, been relatively little study of low and very low audio frequency dispersions in biological membranes containing mixtures of proteins and lipids (see the review by Kell and Harris, 1985) and none in epithelial plasma membranes. Our experiments in frog skin are the first of their kind to evaluate the α-dispersions at the apical membranes of these cells. Since completion of these experiments, α-dispersions have been observed at apical membranes of cell cultured A6 epithelia (Helman et al., 1995; Liu et al., 1995), cell cultured pancreatic ducts (Mangino et al., 1992), and other native tight epithelia (S. I. Helman, unreported observations), so that α-dispersions at the apical membrane of frog skin are not exclusive to this tissue. An ultimate understanding of the origin of α-dispersions is of particular interest in knowing the interactions and arrange-

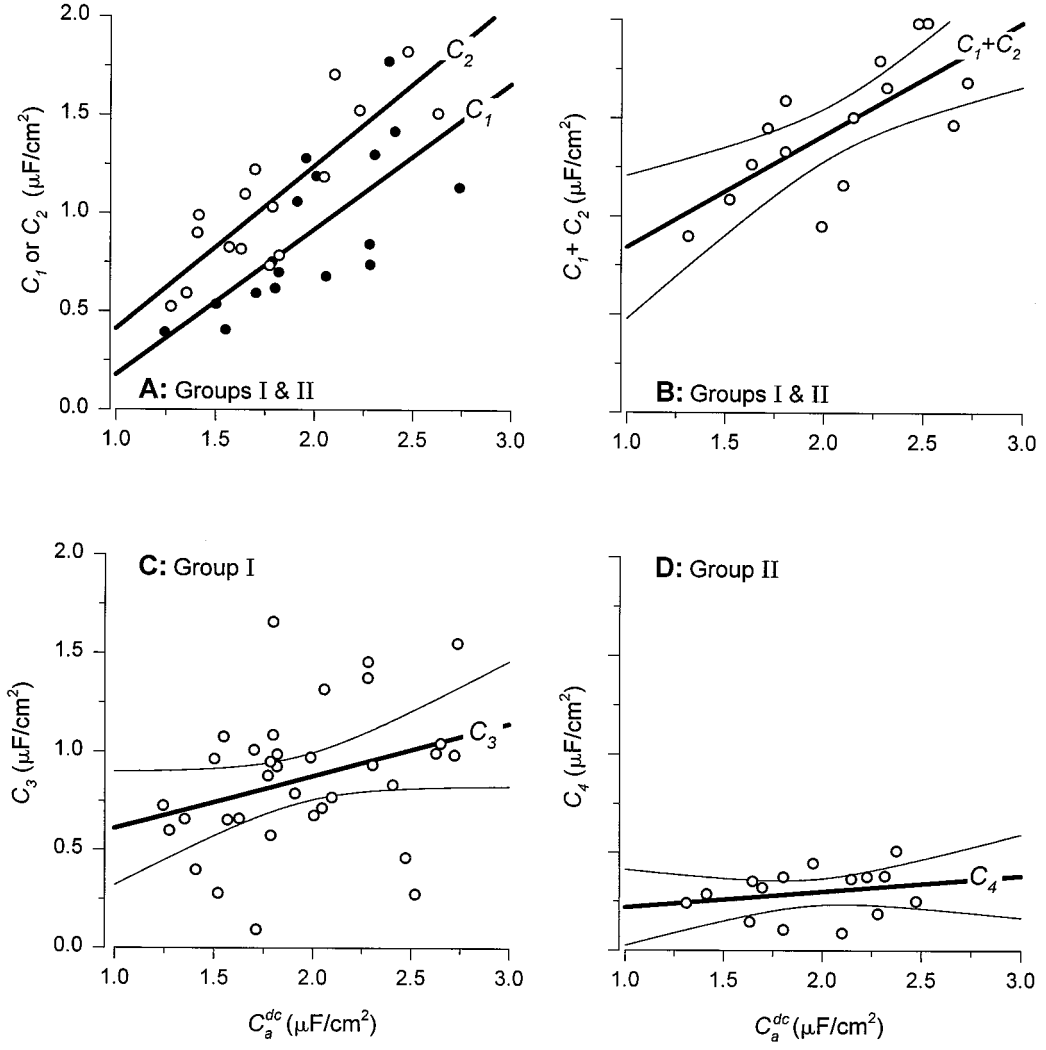

FIGURE 10 Relationships between capacitive increments and the dc capacitance among tissues. Increases in dc capacitance are correlated with increases in either C_1 (groups IA and IIA), C_2 (groups IB and IIB), or $C_1 + C_2$ (groups IC and IIC), as indicated in *A* and *B*. Values of C_1 and C_2 are indicated by solid and open circles, respectively, in *A*. Solid thick lines are the slopes of the respective linear regressions, and thin lines are the 99% confidence interval, where indicated. Confidence intervals are not shown in *A*, to preserve clarity. Neither C_3 (*C*) nor C_4 (*D*) changed significantly with increases in dc capacitance.

ments between the lipids and proteins and their interactions with electrical fields, and the effect of these fields on membrane transport and behavior.

The existence of α-dispersions imposes limitations and complications in the design and interpretation of experiments that use measurements of capacitance as a means of assessing changes in membrane area. We refer in part to our own experiments, which were done to determine whether inhibition of apical membrane Na^+ entry by amiloride caused a change in apical membrane capacitance. It was suggested that amiloride increased C_a (Awayda et al., 1989). We now believe that this suggestion is inconclusive, and we address this issue in the Appendix.

To underscore the issues involved, we illustrate as shown in Fig. 12 for measurements made at a single frequency that increases or decreases in relaxation frequency alone, while all other factors remain the same, give rise to changes in capacitance at the frequency of measurement despite constancy of the dc capacitance, capacitive increments, and membrane area.

We illustrate also in Fig. 13, *A* and *C*, that capacitance per unit planar area can change because of changes in dielectric increments in the absence of change in actual membrane area. In Fig. 13 *A* the changes in C^{dc} are due to changes in the dielectric increment. C_i^{∞}, which is proportional to area, is unchanged. Similarly in Fig. 13 *C*, C^{dc} is increased because of a selective increase in the dielectric increment associated with the C_1 relaxation process. The dielectric increment of the C_2 relaxation process is unchanged, as are the static capacitances C_1^{∞} and C_2^{∞}, which are proportional to area. When changes in area accompany changes in capacitive increments, as illustrated in Fig. 13, *B* and *D*, the C_i^{∞} change together with the C^{dc}. Thus, despite a more extensive description of the relaxation processes at audio and

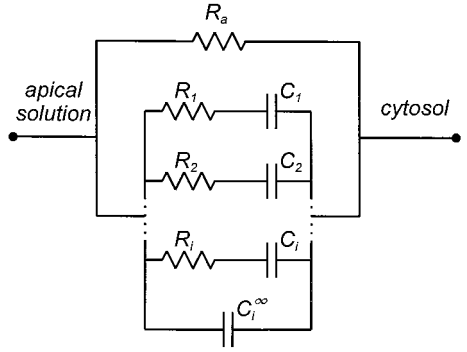

FIGURE 11 Electrical equivalent circuit of apical membrane. R_a is the dc ionic resistance to Na^+ current through epithelial Na^+ channels that are principally amiloride sensitive and some (a few percent) that are amiloride-insensitive. $R_1 \ldots R_i$ are the ac resistances of the relaxation processes with capacitive increments $C_1 \ldots C_i$. Time constants of the relaxation processes are $\tau_i = R_iC_i = (2\pi f_i)^{-1}$. C_i^∞ is the static capacitance associated with the α-relaxation processes at $f \gg f_i$.

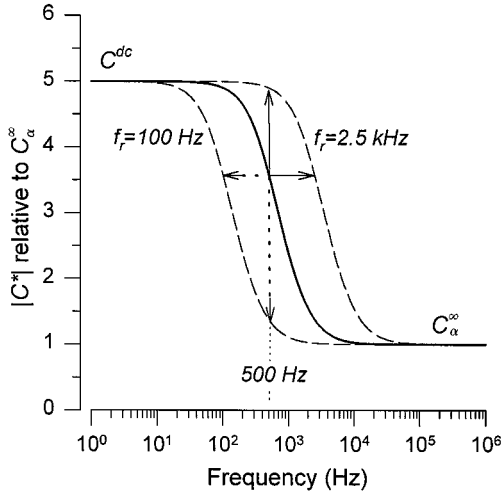

FIGURE 12 When capacitance is measured at a single frequency in the frequency-sensitive range of a relaxation process, changes of capacitance will occur due to changes of relaxation frequency in the absence of change of dc capacitance, capacitive increments and membrane area. For purpose of illustration, the solid line indicates a relaxation process with absolute capacitance that varies between one and five units (dielectric increment of four units) and a relaxation frequency of 500 Hz. If relaxation frequency of of the process decreases to 100 Hz or increases to 2.5 kHz, as indicated by the dashed lines, and capacitance is measured at a constant frequency, then capacitance will decrease or increase as illustrated at a single frequency of 500 Hz despite constancy of C^{dc}, C_α^∞ and the dielectric increment.

higher frequencies as revealed by dielectric spectroscopy, the general problem remains, namely, understanding the origin of changes in capacitance, which are due to changes in either area and/or dielectric increments, where the latter can be altered, for example, by phosphorylation of membrane proteins or lipids or other chemical reactions that do not involve changes in area. We know of no absolute or unequivocal procedure to make this assessment based on capacitance measurements in the audio frequency spectrum, because changes in dielectric increments at higher than audio frequency relaxation processes would result in changes in capacitance at audio frequencies indistinguishable from those due to changes in membrane area. Consequently, it is not possible to know unequivocally whether vesicle trafficking involving membrane insertion and retrieval at the apical membranes of the cells is operative based solely on changes of capacitance. The behavior of the dc capacitance and indeed the capacitance at any frequency in the ranges of α- and β-dispersions may in fact be uncorrelated with changes in membrane area.

It remains of particular interest to know the origin of the audio frequency relaxation processes because, as in frog skin, they dominate in determining the membrane capacitance. In the absence of more detailed information of the content and organization of specific membrane lipids, glycolipids, and integral and surface proteins, and recognizing that biological membranes exhibit a great deal of membrane heterogeneity (Jacobson, 1983; Curtain et al., 1988; Sweet and Schroeder, 1988; van Meer and Simons, 1988; Tocanne et al., 1989; Almeida et al., 1992), it will be of interest to examine other epithelial plasma membranes to characterize their α-dispersions and to determine how best to differentiate between changes of capacitance due to changes in membrane area and changes in dielectric increments.

TABLE 3 R_i^{ac} and ρ_i of relaxation processes

Relaxation process	f_i (Hz)	R_i^{ac} ($\Omega \cdot cm^2$)	ρ_i ($M\Omega \cdot cm$)
f_1	24.8	8,918	17.8
f_2	142	1,121	2.2
f_3	2,085	86.8	0.17
f_4	6,806	80.7	0.16

APPENDIX

Calculation of capacitance assuming frequency-independent dielectrics

If apical and basolateral membrane capacitances are assumed to be frequency independent, the time constants of these membranes are $\tau_a = R_aC_a$ and $\tau_b = R_bC_b$, respectively. Apical (Z_a) and basolateral (Z_b) membrane impedances are then

$$Z_a = \frac{R_a}{1 + (j\omega R_aC_a)^{(1-\alpha)}} \tag{7}$$

$$Z_b = \frac{R_b}{1 + (j\omega R_bC_b)^{(1-\alpha)}} \tag{8}$$

Under ideal conditions where α is zero, Nyquist plots of Z_a or Z_b alone give ideal semicircles, where the time constants can be evaluated from the frequency at the apex of the semicircles. Because Z_a in series with Z_b is paralleled by the shunt resistance, R_p,

$$Z_{meas} - R_{ser} = \frac{(Z_a + Z_b)R_p}{Z_a + Z_b + R_P} \tag{9}$$

If $\tau_a < \tau_b$, a Nyquist plot of Z_{meas} will reflect the existence of two ideal semicircles (shunted by R_p). This is illustrated in Fig. 14 *A* for a control tissue in its Na^+-transporting state before inhibition of Na^+ transport by

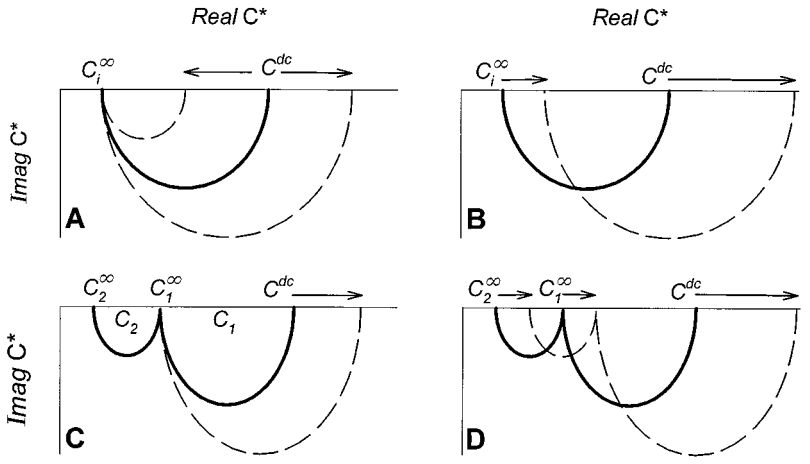

FIGURE 13 Changes in complex capacitance can occur because of changes in membrane area and/or changes in dielectric increments. (*A*) A single relaxation process (*thick solid line*) where, in the absence of change in membrane area, the dc capacitance can either increase or decrease because of change in the dielectric increment without a change in the static capacitance, C_i^{∞}. If changes in the dielectric increment are accompanied by a change in membrane area, C_i^{∞} must also change as indicated in *B*. (*C*) Two relaxation processes (*thick solid line*), where the dc capacitance increases because of a selective increase in the C_1 dielectric increment, with no change in the C_2 dielectric increment or the static capacitances C_1^{∞} and C_2^{∞}. In this case the membrane area is unchanged. If the change in the C_1 dielectric increment is associated with an increase in membrane area, then as indicated in *D*, the static capacitances C_1^{∞} and C_2^{∞} increase together with the dc capacitance.

amiloride and Na^+-free apical solution. The measured dc resistance (R_{meas}^{dc}) was near 3116 $\Omega \cdot cm^2$ in this tissue and averaged 3971 $\Omega \cdot cm^2$ in 23 tissues (Table 4), where

$$R_{meas}^{dc} = \frac{(R_a + R_b)R_p}{R_a + R_b + R_p} + R_{sol} \qquad (10)$$

After inhibition of transport, $R_{meas}^{dc} = R_p + R_{sol}$ increased to a mean value of 23,599 $\Omega \cdot cm^2$, as was illustrated in Fig. 4 and here again in Fig. 14 *B*.

At frequencies less than 50 Hz, the impedance vectors of transport-inhibited tissues conformed to depressed semicircles ($(1 - \alpha) < 1$) as noted above, indicating nonideal behavior of the impedance of the apical membrane of the cells. This was also the case for Na^+-transporting tissues.

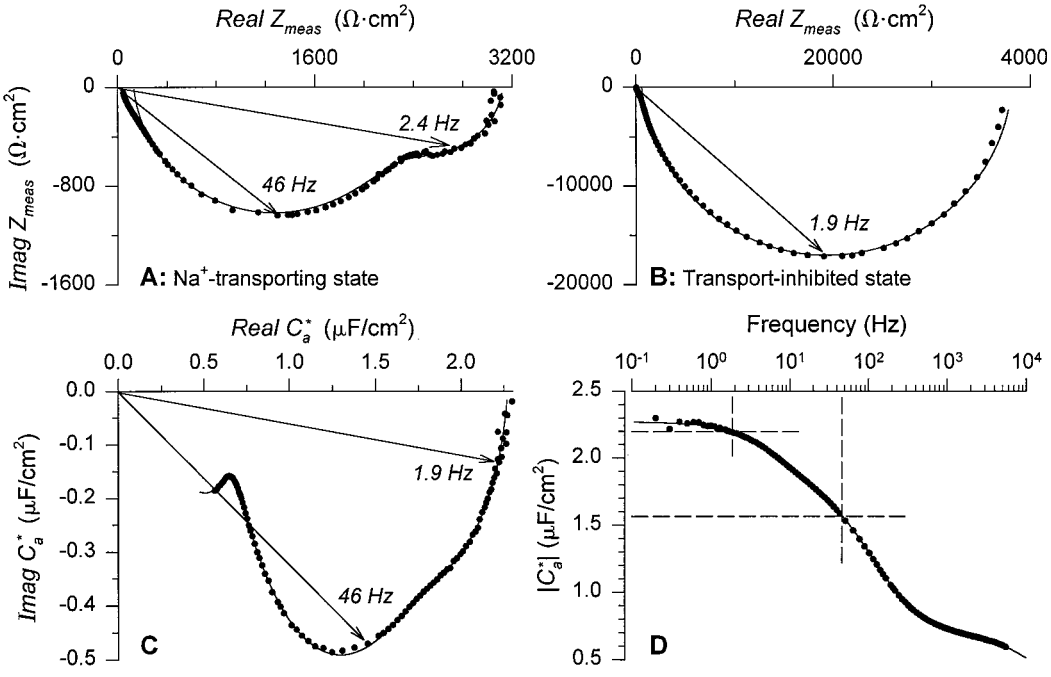

FIGURE 14 Representative example of impedance of isolated epithelium of frog skin measured in its Na^+-transporting (*A*) and transport-inhibited states (*B*). (*A*) The impedance vectors were fit at limited bandwidth to Eq. 8 at frequencies between 0.9 and 269 Hz to resolve the apical and basolateral membrane resistances and capacitances (assuming frequency-independent capacitances). Shunt resistance (R_p = 37.8 k$\Omega \cdot cm^2$) was determined after transport was completely inhibited (*B*). The semicircles representing apical and basolateral membrane impedances were depressed ($(1 - \alpha) = 0.93$), and the frequencies at the apex of the depressed semicircles were 46 and 2.4 Hz, respectively. R_a and R_b were near 2253 and 984 $\Omega \cdot cm^2$. Small improvements of the fit at lower frequencies could be made by further reducing the bandwidth. The extrapolated values of the fitted curves to the real axis at infinite frequency (R_{ser}; Table 4) markedly overestimated the R_{ser}. (*C*) Complex capacitance of apical membrane exhibiting three relaxation processes. Capacitance vectors at 1.9 and 46 Hz correspond to the frequencies at which apical membrane capacitance was calculated in the transport-inhibited and transporting states of the tissue, respectively. (*D*) Dependence of absolute magnitude of the apical membrane complex capacitance on frequency. The intersections of the dashed lines indicate the magnitudes of capacitance at 1.9 and 46 Hz.

TABLE 4 Calculations of apical and basolateral membrane capacitance assuming frequency independence

Tissue	R^{dc}_{meas} ($\Omega \cdot cm^2$)	R_{ser} ($\Omega \cdot cm^2$)	R_a ($\Omega \cdot cm^2$)	C_a ($\mu F/cm^2$)	R_b ($\Omega \cdot cm^2$)	C_b ($\mu F/cm^2$)	$(1 - \alpha)$
Na^+-transporting tissues ($n = 23$)	3,971 ± 285	106 ± 8	3,803 ± 386	1.52 ± 0.058	1,211 ± 109	68.5 ± 6.2	0.915 ± 0.006
Transport-inhibited tissues ($n = 33$)	23,599 ± 2,616	405 ± 31	∞	1.84 ± 0.066	—	—	0.945 ± 0.003

Values are means ± SE.

Nonlinear curve fits of the impedance vectors to Eq. 8 at bandwidths less than a few hundred hertz gave values of $1 - \alpha$ that averaged 0.915 for the Na^+-transporting state of the tissues and 0.945 for the transport-inhibited state of the tissues (Table 4). R_a and R_b averaged 3803 and 1211 $\Omega \cdot cm^2$, yielding a fractional transcellular resistance $fR_a = R_a/(R_a + R_b)$ of 0.758, which is fairly typical of those reported previously for the Na^+-transporting state of the tissues (Helman and Fisher, 1977; Fisher et al., 1980; Helman and Thompson, 1982). C_a and C_b averaged 1.52 and 68.5 $\mu F/cm^2$. In the transport-inhibited state, C_a averaged 1.84 $\mu F/cm^2$, suggesting that apical membrane capacitance is increased by inhibition of Na^+ entry at the apical membranes of the cells (Awayda et al., 1989).

Taken at face value, the values of capacitance calculated above would seem reasonable and are in the range expected for the epithelium of frog skin, where because of the functional electrical coupling of the multicellular layers of basolateral membranes, C_b is expected to be considerably larger than C_a. Recognizing that the contribution of C_b to the impedance is dominant at the lowest frequencies of a few hertz, the C_b so calculated should closely approach the dc capacitance of the basolateral membranes (C^{dc}_b), provided that dielectric dispersions at basolateral membranes exist at much higher frequencies, as they do at the apical membranes. Because the impedance of the basolateral membranes becomes insignificant relative to the impedance of the apical membranes at higher frequencies, it remains impossible at present to know if basolateral membranes exhibit α-dielectric dispersions. Accordingly, it also remains impossible to know whether changes in C^{dc}_b reflect changes in basolateral membrane area and/or changes in dielectric increments.

Does inhibition of apical membrane Na^+ entry cause an increase in C_a?

Although the values of C_a calculated as indicated above appear reasonable, it must be recalled that C_a are calculated assuming frequency independence and in a range of frequency where our analysis indicated the existence of large α-dispersions. For the experiment shown in Fig. 14, the frequency at the apex of the apical membrane depressed semicircle was 46 Hz in the Na^+-transporting state (Fig. 14 *A*) and 1.9 Hz in the transport-inhibited state (Fig. 14 *B*) of the tissue. The complex capacitance of the apical membrane shown in Fig. 14 *C* exhibited three relaxation processes at audio frequencies. The capacitance vectors are labeled at 1.9 and 46 Hz, corresponding to the frequencies at which the C_a was calculated above assuming frequency independence. As indicated in Fig. 14 *D*, the absolute value of complex capacitance decreases with increasing frequency from a dc capacitance near 2.3 $\mu F/cm^2$. At 1.9 and 46 Hz, the capacitances are 2.19 and 1.57 $\mu F/cm^2$, respectively. Thus, in addition to actual changes in capacitance that may or may not have occurred because of inhibition of transport, the assumption of a frequency-independent capacitance does not take into account a change in capacitance due to frequency-dependent changes in the membrane dielectric and the frequency at which capacitance is calculated. Accordingly, for the particular case where epithelia are very tight and where inhibition of Na^+ entry leads to large increases in transepithelial resistance and hence decreases in the characteristic frequency at which capacitance is calculated, the observation of increases in capacitance like those indicated above may in fact be misleading and certainly biased toward a false conclusion. It therefore remains unknown whether amiloride inhibition of transport causes changes in C^*_a.

A similar argument would pertain to the case where, for example, the shunt resistance changes in the absence of any change in resistance and capacitance at apical and basolateral membranes of the cells that would lead to a change in the time constants and characteristic frequencies at which capacitance is calculated. We have found this pitfall to be pertinent in our own studies of frog skin, underscoring the need to evaluate the dielectric properties of native plasma membranes for the existence of α-dispersions.

We gratefully acknowledge financial support from the University of Illinois at Urbana-Champaign Campus Research Board to SIH and National Institutes of Health DK 30824 to SIH. MSA received support from National Institutes of Health training grant GM 7143 while a graduate student and doctoral candidate in the Department of Physiology and Biophysics at the University of Illinois. SIH received fellowship support from the Katholieke Universiteit Leuven Research Council during the summer of 1990 while collaborating in research on this project in Leuven, Belgium, with W. Van Driessche.

REFERENCES

Abramcheck, F. J., W. Van Driessche, and S. I. Helman. 1985. Autoregulation of apical membrane Na^+ permeability of tight epithelia. Noise analysis with amiloride and CGS 4270. *J. Gen. Physiol.* 85:555–582.

Almeida, P. F. F., W. L. C. Vaz, and T. E. Thompson. 1992. Lateral diffusion in the liquid phases of dimyristoylphosphatidylcholine/cholesterol lipid bilayers: a free volume analysis. *Biochemistry.* 31: 6739–6747.

Armstrong, C. M., and F. Bezanilla. 1975. Currents associated with the ionic gating structures in nerve membrane. *Ann. N.Y. Acad. Sci.* 264: 265–277.

Awayda, M. S., and S. I. Helman. 1990. Absence of change of apical membrane capacitance with forskolin stimulation of Na transport in frog skin. *FASEB J.* 4:A550 (Abstr.).

Awayda, M. S., and S. I. Helman. 1992. Na^+ transport related changes of apical membrane capacitance in the tight epithelium of frog skin. *FASEB J.* 6:A1239 (Abstr.).

Awayda, M., W. Van Driessche, and S. I. Helman. 1989. Impedance analysis of apical and basolateral membranes of epithelial cells of frog skin. *FASEB J.* 3:A982 (Abstr.).

Awayda, M. S., W. Van Driessche, and S. I. Helman. 1991. Frequency-dependent complex dielectric properties of an epithelial plasma membrane. *Biophys. J.* 59:28a (Abstr.).

Bao, J.-Z., C. C. Davis, and R. E. Schmukler. 1992. Frequency domain impedance measurements of erythrocytes. Constant phase angle impedance characteristics and a phase transition. *Biophys. J.* 61:1427–1434.

Cole, K. S. 1968. Membranes, Ions and Impulses. University of California Press, Berkeley, CA.

Cole, K. S., and R. H. Cole. 1941. Dispersion and absorption in dielectrics. I. Alternating current characteristics. *J. Chem. Phys.* 9:341–351.

Coster, H. G. L., and J. R. Smith. 1974. The molecular organisation of bimolecular lipid membranes. A study of the low frequency Maxwell-Wagner impedance dispersion. *Biochim. Biophys. Acta.* 373:151–164.

Curtain, C. C., L. M. Gordon, and R. C. Aloia. 1988. Lipid domains in biological membranes: conceptual development and significance. *In*

Lipid Domains and the Relationship to Membrane Function. R. C. Aloia, C. C. Curtain, and L. M. Gordon, editors. Alan R. Liss, New York. 1–15.

Daniel, V. V. 1967. Dielectric Relaxation. Academic Press, London.

Debye, P. 1929. Polar Molecules. Chemical Catalog Co., New York.

Fisher, R. S., D. Erlij, and S. I. Helman. 1980. Intracellular voltage of isolated epithelia of frog skin. Apical and basolateral cell punctures. *J. Gen. Physiol.* 76:447–453.

Foster, K. R., and H. P. Schwan. 1989. Dielectric properties of tissues and biological materials: a critical review. *CRC Crit. Rev. Biomed. Eng.* 17:25–104.

Fricke, H., and S. Morse. 1925. The electric resistance and capacity of blood for frequencies between 800 and 4 1/2 million cycles. *J. Gen. Physiol.* 9:153–167.

Gabler, R. 1978. Electrical Interactions in Molecular Biophysics. Academic Press, New York.

Hanai, T., D. A. Haydon, and J. Taylor. 1964. An investigation by electrical methods of lecithin-in-hydrocarbon films in aqueous solutions. *Proc. R. Soc. Lond. A.* 281:377–391.

Hanai, T., D. A. Haydon, and J. Taylor. 1965. The influence of lipid composition and of some adsorbed proteins on the capacitance of black hydrocarbon membranes. *J. Theor. Biol.* 9:422–432.

Helman, S. I., and R. S. Fisher. 1977. Microelectrode studies of the active Na transport pathway of frog skin. *J. Gen. Physiol.* 69:571–604.

Helman, S. I., X. Liu, and W. J. Els. 1995. Vesicle trafficking and aldosterone-stimulated Na^+ transport in A6 epithelia. *J. Gen. Physiol.* 105:42a (Abstr.).

Helman, S. I., and S. M. Thompson. 1982. Interpretation and use of electrical equivalent circuits in studies of epithelial tissues. *Am. J. Physiol.* 243:F519–F531.

Jacobson, K. 1983. Lateral diffusion in membranes. *Cell Motil.* 3:367–373.

Jonscher, A. K. 1983. Dielectric Relaxation in Solids. Chelsea Dielectrics Press, London.

Kell, D. B., and C. M. Harris. 1985. On the dielectrically observable consequences of the diffusional motions of lipids and proteins in membranes. 1. Theory and overview. *Eur. Biophys. J.* 12:181–197.

Liu, X., W. J. Els, and S. I. Helman. 1995. Aldosterone increases apical membrane capacitance of A6 epithelia. *FASEB J.* 9:A64 (Abstr.).

Mangino, M. M., M. S. Awayda, and S. I. Helman. 1992. Secretin stimulated apical chloride conductance and vesicle fusion in cultured pancreatic duct cells. *FASEB J.* 6:A1238 (Abstr.).

Mărgineanu, D.-G., and W. Van Driessche. 1990. Effects of millimolar concentrations of glutaraldehyde on the electrical properties of frog skin. *J. Physiol. (Lond.).* 427:567–581.

Pethig, R. 1979. Dielectric and Electronic Properties of Biological Materials. John Wiley and Sons, New York.

Schwan, H. P. 1957. Electrical properties of tissue and cell suspensions. *In* Advances in Biological and Medical Physics, Vol. V. J. H. Lawrence and C. A. Tobias, editors. Academic Press, New York. 147–209.

Schwan, H. P., and K. R. Foster. 1980. RF-field interactions with biological systems: electrical properties and biophysical mechanisms. *Proc. IEEE.* 68:104–113.

Sweet, W. D., and F. Schroeder. 1988. Lipid domains and enzyme activity. *In* Lipid Domains and the Relationship to Membrane Function. R. C. Aloia, C. C. Curtain, and L. M. Gordon, editors. Alan R. Liss, New York. 17–42.

Takashima, S. 1989. Electrical Properties of Biopolymers and Membranes. Adam Hilger, Bristol.

Tang, J., F. J. Abramcheck, W. Van Driessche, and S. I. Helman. 1985. Electrophysiology and noise analysis of K^+-depolarized epithelia of frog skin. *Am. J. Physiol. Cell Physiol.* 249: C421–C429.

Tocanne, J.-F., L. Dupou-Cezanne, A. Lopez, and J.-F. Tournier. 1989. Lipid lateral diffusion and membrane organization. *FEBS Lett.* 257: 10–16.

Van Driessche, W. 1986. Lidocaine blockage of basolateral potassium channels in the amphibian urinary bladder. *J. Physiol. (Lond.).* 381: 575–593.

van Meer, G., and K. Simons. 1988. Lipid polarity and sorting in epithelial cells. *J. Cell. Biochem.* 36:51–58.

Watanabe, M., T. Suzaki, and A. Irimajiri. 1991. Dielectric behavior of the frog lens in the 100 Hz to 500 MHz range. Simulation with an allocated ellipsoidal-shells model. *Biophys. J.* 59:139–149.

White, S. H., and T. E. Thompson. 1973. Capacitance, area, and thickness variations in thin lipid films. *Biochim. Biophys. Acta.* 323:7–22.